Accelerated improvement in tensile superelasticity of electron beam directed energy deposition manufactured NiTi alloys by artificial thermal cycling combined with low temperature aging treatment

Ze Pu, Changyong Chen, Dong Du, Rui Xi, Hao Jiang, Kaiming Wang, Liying Sun, Xiebin Wang & Baohua Chang

Taylor & Francis
Taylor & Francis Group

Accelerated improvement in tensile superelasticity of electron beam directed energy deposition manufactured NiTi alloys by artificial thermal cycling combined with low temperature aging treatment

Ze Pu[a,b], Changyong Chen[b], Dong Du[a], Rui Xi[c], Hao Jiang[c], Kaiming Wang[d], Liying Sun[e], Xiebin Wang[c] and Baohua Chang[a]

[a]State Key Laboratory of Tribology in Advanced Equipment, Department of Mechanical Engineering, Tsinghua University, Beijing, People's Republic of China; [b]Research Institute for Advanced Manufacturing, Department of Industrial and Systems Engineering, The Hong Kong Polytechnic University, Hong Kong, People's Republic of China; [c]Key Laboratory for Liquid–Solid Structural Evolution and Processing of Materials (Ministry of Education), Shandong University, Jinan, People's Republic of China; [d]College of Automotive and Mechanical Engineering, Changsha University of Science and Technology, Changsha, People's Republic of China; [e]Institute of New Materials, Guangdong Academy of Sciences, Guangzhou, People's Republic of China

ABSTRACT

The low-temperature aging treatment at 250°C can significantly improve the tensile superelasticity of NiTi alloys fabricated by electron beam directed energy deposition (EB-DED). However, it requires a very long aging duration (up to 200 h) to achieve excellent tensile superelasticity due to inherent coarse grain size. To accelerate the aging process, the high-density dislocations are introduced by artificial thermal cycling treatment prior to the aging treatment (the original dislocation content in EB-DED processed NiTi alloys is very low), which will promote the subsequent uniform precipitation of nanoscale Ni_4Ti_3 particles during low-temperature aging treatment. The phase transformation behaviour always maintains a stable two-stage martensitic phase transformation. Under a cyclic tensile test at 6% strain, 24 h aged sample with thermal cycling maintains a recovery rate exceeding 90% even after 10 cycles, comparable to the performance of the sample aged for 200 h without thermal cycling, indicating a substantial improvement in aging efficiency.

1. Introduction

NiTi shape memory alloys exhibit excellent functional properties (shape memory effect and superelasticity), corrosion resistance, biocompatibility and mechanical properties [1–4], making it one of the most promising shape memory alloys, and have broad application prospects in various fields [5]. In recent years, the preparation of NiTi alloys based on additive manufacturing (AM) has attracted significant attention [6,7], because its layer-by-layer printing strategy gives great freedom to fabricate highly customised complex structures [8,9], and circumvents the common challenges in processing NiTi alloys by conventional approaches, such as machining and welding [10,11]. Consequently, the emergence and development of additive manufacturing technology have greatly broadened the application scenarios of NiTi alloys.

For additively manufactured NiTi alloy components, it's crucial to ensure the required functional properties while meeting the structural requirements [12]. However, current research shows that the functional properties of additively manufactured NiTi alloys are often unsatisfactory in their as-built state without any post treatment [13,14]. Particularly, the tensile superelasticity is much worse than that of conventional NiTi alloys. In general, since the stress required to trigger the superelasticity is higher than that for shape memory effect, achieving superelasticity is more difficult and requires higher matrix strength for NiTi alloys [1]. Moreover, the tensile test mode is more sensitive to the structural defects (e.g. pores and cracks) than other deformation mode [15]. Therefore, it is relatively challenging to achieve ideal tensile superelasticity for additively manufactured NiTi alloys.

According to the previous studies on NiTi alloys, the excellent superelasticity can be achieved by two kinds of technical routes [16–18]. The first is grain refinement

normally through severe plastic deformation (e.g. cold drawing, cold rolling, equal channel angular extrusion, high-pressure torsion) [19,20]. When the grains are refined to nano-size, especially less than 100 nm, the functional stability could be significantly improved [21]. Moreover, if the grains are too fine (less than 50 nm), the martensite phase transformation would be remarkably suppressed, leading to the change of typical superelastic response with transformation plateaus to linear-elasticity [22]. Constrained by the additive manufacturing process and the material characteristics of NiTi alloy, the grains of additively manufactured NiTi alloys are generally at the level of several ten microns or above [6,23–26]. However, the additively manufactured NiTi alloy components having already been formed into final shapes cannot experience severe plastic deformation. Therefore, the grain refinement seems to be not applicable for additively manufactured NiTi alloys.

The second technical route is precipitation hardening by introducing Ni_4Ti_3 particles through appropriate aging treatment. The effectiveness of precipitation hardening strictly depends on the size, distribution and density of Ni_4Ti_3 precipitates in NiTi alloys [17,27,28]. Although some studies have reported the inherent formation of Ni_4Ti_3 particles in additively manufactured NiTi alloys [25,29–31], the layer-by-layer printing strategy of additive manufacturing leads to varying thermal histories at different locations, making it challenging to control the size and distribution of Ni_4Ti_3 formed during additive manufacturing process. Previous studies have found that the nano-sized (<15 nm) and densely dispersed Ni_4Ti_3 could be introduced through low temperature aging treatment (200–300°C) and act as effective obstacles to the movement of dislocations and well improve the performance of superelasticity [17,28]. Clearly, for additively manufactured NiTi alloys, low temperature aging treatment is a good approach to improve the superelasticity.

Among various additive manufacturing processes, electron beam directed energy deposition (EB-DED) is advantageous for fabricating dense structures without oxidation, working in a vacuum environment and using wire as feedstock, and is considered as a reliable technique for producing high-performance NiTi alloy components [24,32–34]. However, due to the coarse grain size (up to a few hundred microns) and lack of effective strengthening phase, the superelasticity at as-built state is not satisfactory. Our previous work has systematically investigated the influence of different aging temperatures and times on the improvement of superelasticity [35]. It was found that aging at a low temperature at 250°C is very safe, as at this temperature the

size of the precipitated Ni_4Ti_3 particles will not become excessively large. Moreover, the operating temperature for superelasticity is near room temperature, which holds great value for practical applications. With prolonged aging times (within 200 h), the superelasticity can be gradually improved. After aging at 250°C for 200 h, a recovery rate of approximately 90% can be maintained in 10 superelastic cycles at 6% tensile strain, which is quite good superelasticty exhibited by additively manufactured NiTi alloys. However, due to the coarse grain size caused by the poor heat dissipation in vacuum chamber, the precipitation process during low temperature aging is slow, requiring a long time to achieve satisfactory performance.

Inspired by the classical solid-state phase transformation theory, dislocations may act as heterogeneous nucleation sites to promote the precipitation [36]. While the dislocations could be introduced into NiTi alloys during thermal-induced martensitic phase transformation [37]. In this paper, we aim to introduce high-density dislocations into the EB-DED manufactured NiTi alloy prior to low temperature aging treatment through artificial thermal cycling treatment, in which the temperature range could fully cover the austenitic and martensitic phase transformation temperatures and thus induce repeated phase transformations between austenite and martensite. Therefore, with the assistance of high-density dislocations, the efficiency of low temperature aging treatment is expected to be improved.

2. Experimental procedure

2.1. EB-DED process conditions

In this work, a multilayer NiTi alloy wall part was fabricated by a wire-based electron beam directed energy deposition machine (Figure 1(a)) using a commercial Ti-50.8 at.% Ni alloy wire with a diameter of 2 mm as feedstock. The process worked in a vacuum chamber with a pressure below 4×10^{-2} Pa. Figure 1(b) shows the schematic diagram of EB-DED process. A rolled Ti-50.8 at.% Ni alloy plate with dimensions of 2mm × 10mm × 200 mm was used as the substrate and no pre-heating was employed in the substrate. The key process parameters of EB-DED used in this work could guarantee a good forming quality and less Ni-evaporation: acceleration voltage of 60 kV, beam current of 40 mA, wire feeding speed of 1200 mm/min, and substrate moving speed of 300 mm/min. The deposition path was configured as a reciprocating single pass and the layer thickness was set to 1 mm. Figure 1(c) shows the morphology of the as-built wall-structured NiTi alloy part.
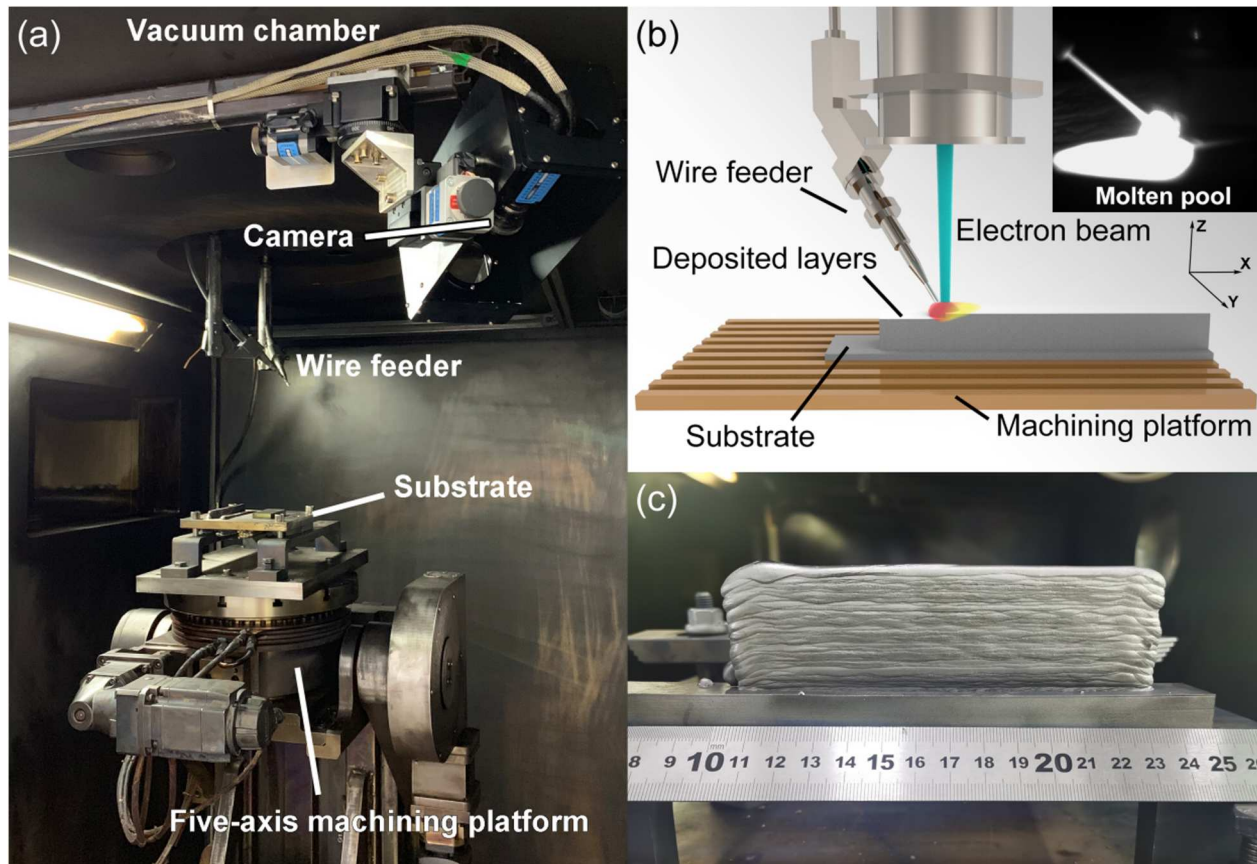
Figure 1. (a) Wire-based electron beam directed energy deposition machine; (b) the schematic diagram of electron beam directed energy deposition process; (c) the morphology of the as-built wall-structured NiTi alloy part.

2.2. Heat treatment methods

Three types of heat treatment methods were employed in this work. The first is solution treatment, which was conducted at 700°C for 1 h to promote the microstructural homogeneity of the fabricated NiTi part. The artificial thermal cycling treatment is performed by alternatively put the samples in hot environment (90°C water in a thermostatic bath, completely immerse for 3 min) and cold environment (liquid nitrogen, completely immerse for 3 min). The temperature of hot environment is much higher than the austenite transformation finish temperature (Af) of as-built NiTi alloy part. The temperature of cold environment is much lower than the martensite transformation finish temperature (Mf). One thermal cycle is defined as one sequence of 'hot-cold-hot', meaning the sample experienced a phase transformation process of 'austenite-martensite-austenite'. 50 thermal cycles (50TC) were conducted in this work, which took about 6 h, ignoring the time taken for transferring the samples. The low temperature aging treatment at 250°C for durations ranging from 1 to 200 h was conducted to study the improvement in tensile superelasticity. Moreover, the high temperature aging

treatment at 450°C was also carried out for comparison in this study. All the solution treatment and aging treatment in this work were performed in a tube furnace protected by Ar gas flow, followed by quick water quenching.

2.3. Microstructural and thermomechanical characterisation

The microstructural characterisation of EB-DED processed NiTi alloy part was conducted using the optical microscope (OM, OLYMPUS BX51), scanning electron microscope (SEM, ZEISS GeminiSEM 300) and transmission electron microscope (TEM, Tecnai F30). Samples for the OM and SEM observations were mechanically polished and etched using 10 vol.% HF: 40 vol.% HNO3: 50 vol.% H2O solution. A GATAN 691 precision ion polishing system was utilised to prepare TEM samples. The phase transformation behaviour was investigated by Differential scanning calorimetry (DSC, NETZSCH DSC 204) at a heating/cooling rate of 10°C/min between −150°C and 150°C. Cyclic tensile superelastic test to a constant strain of 6% with a strain rate of 3 ×

10^{-4} s^{-1} was performed on a Zwick/Roell Z020 electronic universal testing machine equipped with a temperature control chamber. Samples for superelastic tests have dimensions of 15 mm(X) $\times$ 2 mm(Z) $\times$ 0.8 mm(Y), extracted from the middle part of the as-built NiTi structure. The tensile direction is perpendicular to the building direction. All aged samples are tested at a temperature of 35°C.

3. Results

3.1. Microstructure

The grain morphology of EB-DED processed NiTi alloys is shown in Figure 2. From the OM image constructed for the Y-Z section (Figure 2(a)), it is evident that the as-built NiTi alloys exhibits coarse columnar grains continuously along the building direction and many grains almost completely traverse the whole building height of 45 mm. The formation of these columnar grains is attributed to the maximum heat dissipation direction along the building direction and the epitaxial growth phenomenon during EB-DED process [33]. Furthermore, the grain width exhibits a gradual increase with the building height, due to the poorer cooling speed at higher positions. At the top region, the size of columnar grains is very large and some of them even exceed 1000 μm (Figure 2(b, c)). The columnar grains in the middle region are smaller than those at the top region, with a width of around 500 μm (Figure 2(d, e)). There is a transition in grain morphology at the bottom region of the sample (Figure 2(f, g), where the NiTi alloy substrate shows equiaxed grains and the deposited NiTi alloy sample exhibits columnar grains, which have a width of approximately 200 μm.

The artificial thermal cycling treatment is applied to introduce dislocations into the EB-DED prepared NiTi alloys. As schematically shown in Figure 3(a), when the sample is maintained in the 90°C water (hot environment), which exceeds its Af, it ensures that the sample is in a fully austenitic state (B2). When the sample is placed in the cold environment of liquid nitrogen, significantly below its Mf, the matrix will be in a fully martensitic state (B19'). The rapid thermal-induced martensitic phase transformation achieved by alternating between the hot and cold environments results in fast movement of the austenite-martensite phase interface. The dislocations will be formed and remained during the phase interface movement.
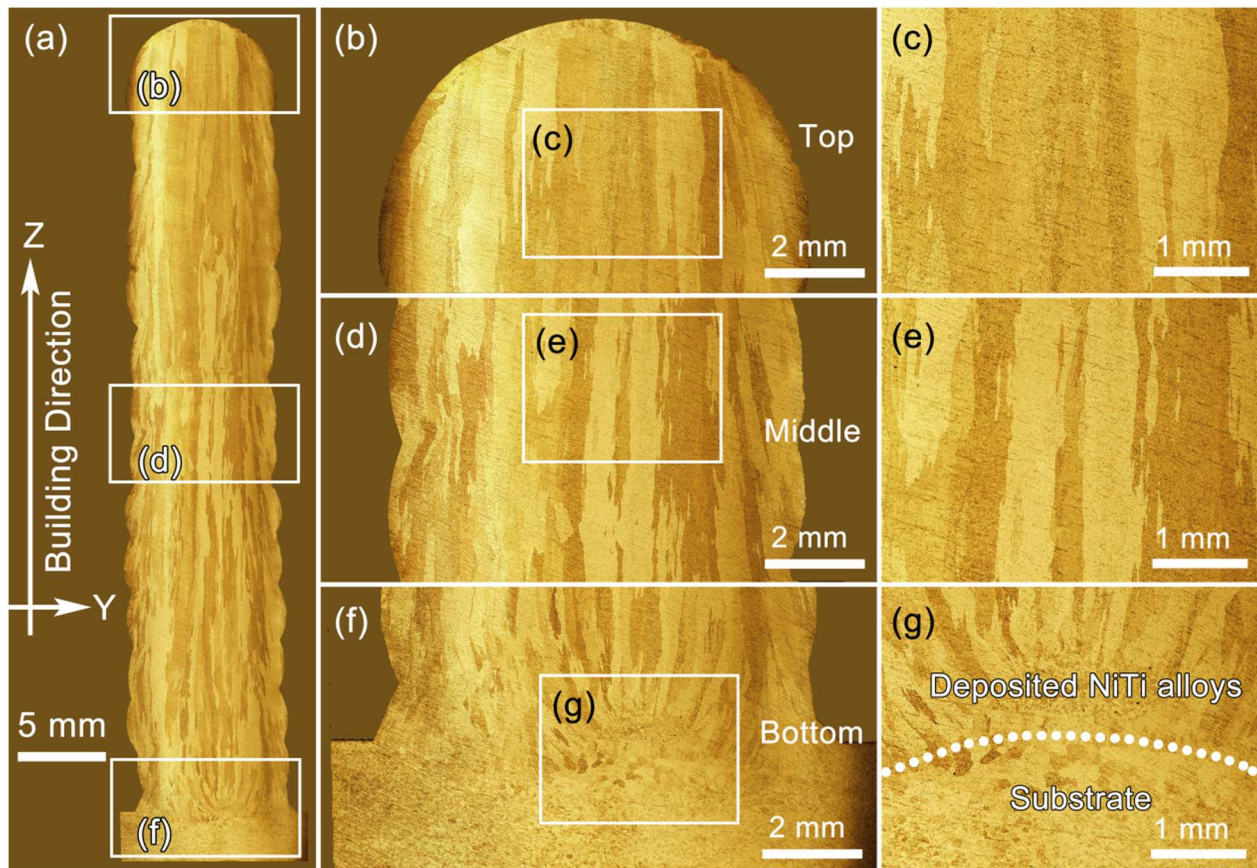

Figure 2. Optical micrograph images of as-built NiTi alloys observed on the Y-Z cross section (along the building direction).
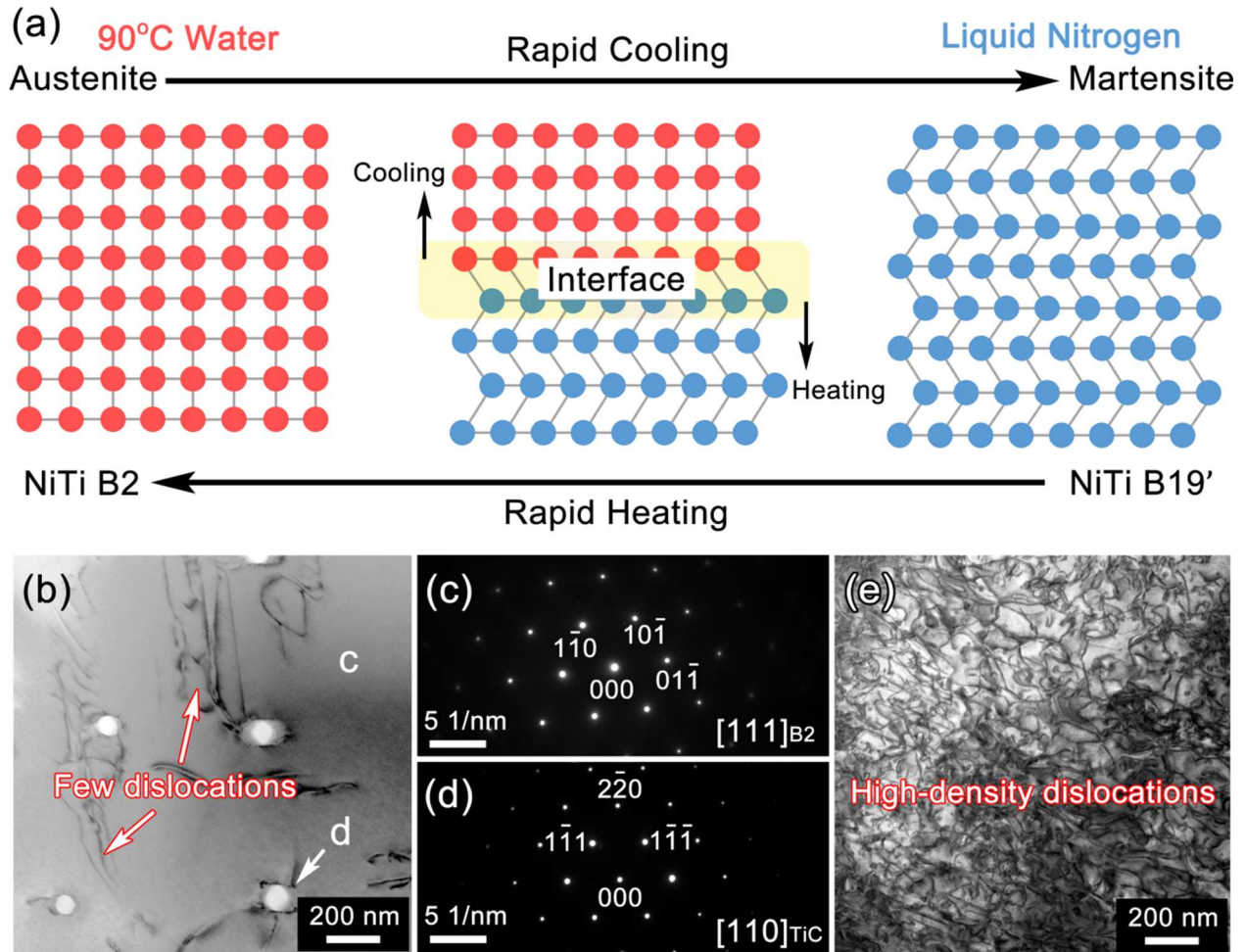
Figure 3. (a) Schematic diagram of artificial thermal cycling treatment conducted between 90°C water and liquid nitrogen; (b) TEM image of as-built NiTi alloys; SAED patters of (c) B2 matrix and (d) TiC phase; (e) TEM image of high-density dislocations in NiTi alloys after 50 times thermal cycling treatment.

At as-built state, the EB-DED processed NiTi alloy sample exhibits a low dislocation content, as shown in the TEM bright-field image of Figure 3(b). The matrix is in austenite state (Figure 3(c)), and dislocations are primarily present near the TiC particles (Figure 3(d)). After 50 times thermal cycling treatment, a high density of tangled dislocations can be observed under TEM (Figure 3(e)), indicating a significant increase in dislocation density within the matrix by the thermal cycling treatment.

3.2. Phase transformation behaviour

According to the DSC curves in Figure 4, the as-built NiTi sample exhibits a typical one-step martensitic transformation, displaying an A→M transformation during cooling process with a Mp of −19°C and a M→A transformation during heating process with an Ap of 6°C. After undergoing 50 thermal cycles, the DSC curve shifts to the left (lower temperature) side. During the cooling

process, a weak R-phase transformation peak (R→M) emerges, while the B19' transformation peak is suppressed. As a result, the Mp decreases to −35°C.
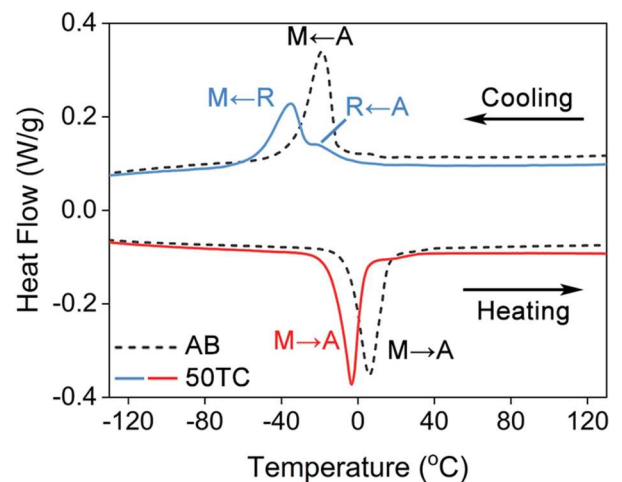

Figure 4. Phase transformation behaviour of NiTi alloys at as-built (AB) state and after 50 thermal cycles (50TC).

During the heating process, only the M→A transformation presents, but the Ap temperature also decreases to −3℃.

The phase transformation behaviour of 50TC samples subjected to low temperature aging at 250℃ for different durations are shown in Figure 5. Additionally, the results for corresponding samples aged without prior thermal cycling treatment are also provided for intuitive comparison. According to Figure 5(a), after aging for 1 h, the 0TC sample still shows a one-step martensitic transformation, with no significant change in transformation sequence. However, the 50TC sample, after a 1-h aging, displays a two-stage martensitic transformation during the cooling process, including an intermediate R-phase transformation peak. Moreover, the B19′ phase transformation peak notably shifts to the left side, decreasing to −41℃. During the heating process, there is a tendency to show a R-phase transformation peak.

As shown in Figure 5(b), after 4 h of aging, the overall phase transformation behaviour of 0TC sample still has no obvious change. For 4 h aged 50TC sample, the transformation behaviour during the cooling process does not exhibit noticeable change. However, during the heating process, a more distinct R-phase transformation peak appears.

After prolonging the aging time to 8 h (Figure 5(c)), the 0TC sample begins to exhibit a two-stage transformation sequence, with a weak one-step R-phase transformation during the cooling process. However, during the heating process, it still shows a one-step M→A transformation. The 50TC sample after aging for 8 h shows a two-stage transformation sequence, including one-stage R-phase transformation, during both the cooling and heating processes. The B19′ transformation in 8 h aged 50TC sample is significantly suppressed during the cooling process, with Mp dropping sharply to −64℃. The gap between Mp and Rp significantly increases. During the heating process, a distinct and independent R-phase transformation peak occurs followed by the R→A transformation with the temperature increases.

When extending the aging time from 8 to 12 h (Figure 5(d)), the phase transformation behaviour of both the 0TC and 50TC samples has no significant change. After aging for 24 h, as presented in Figure 5(e), the 0TC sample exhibits further change in its phase transformation behaviour, showing a three-stage martensitic transformation during both cooling and heating processes, including two R-phase transformation peaks. During the cooling process, as the temperature decreases, it sequentially shows a transformation sequence of A→R1, A→R2, and R→M. Moreover, the Mp is suppressed to −45℃. During the heating

process, with the increase of temperature, it shows the transformation sequence of M→R, R2→A, and R1→A. However, the transformation sequence and temperatures of the 24 h aged 50TC sample does not show significant changes when increasing the aging time.

After 48 h of aging (Figure 5(f)), the 0TC sample still exhibits similar three-stage martensitic transformation behaviour as the 24 h aged sample, while the Mp is further decreased to −50℃. For 48 h aged 50TC sample, it still exhibits a stable two-stage martensitic transformation behaviour in both cooling and heating processes.

Upon extending the aging time to 100 h (Figure 5(g)), it can be observed that the phase transformation sequence of the 0TC sample changes to a two-stage process. The previous two-step R-phase transformation consolidates into a one-step R-phase transformation, which is essentially consistent with the behaviour of the 100 h aged 50TC sample. Subsequently, the phase transformation behaviours of the 0TC and 50TC samples begin to stabilise and have no obvious change after 200 h of aging (Figure 5(h)).

3.3. Tensile superelasticity

Figure 6 shows that the as-built NiTi alloy sample exhibits poor superelasticity. After the first cyclic test to a constant tensile strain of 6%, sample has a residual strain of 3.46%, with a recovery rate of only 42.33% after the first cycle. After 10 cycles, the accumulated residual strain increases to 3.99%, with a recovery rate of 33.50%. After 50 thermal cycles, the superelasticity of the sample shows a noticeable change, exhibiting slight improvement compared to the as-built state. In the first cycle, the critical stress for stress-induced martensitic transformation significantly increases from 285 to 459 MPa and the residual strain decreases to 2.06%, with a recovery rate of 65.67%. After 10 cycles, the residual strain is 2.89%, with a recovery rate of 51.83%.

Figure 7 presents the tensile superelastic curves of 50TC samples after aging at 250℃ for various durations. The aged samples without thermal cycling treatment are also included in the Figure 7 for intuitive comparison. Besides, the accumulated residual strain and the incremental residual strain in each cycle for all aged samples are summarised in Figure 8.

After aging for 1 h, the superelasticity of 0TC sample has no significant change (Figure 7(a*)). A considerable residual strain of 3.32% is generated in the first cycle, with a recovery rate of less than 50%. After 10 cycles, the accumulated residual strain increases to 3.83%, and the recovery rate decreases to 36.17%. As shown in Figure 7(a), the 50TC sample demonstrates an
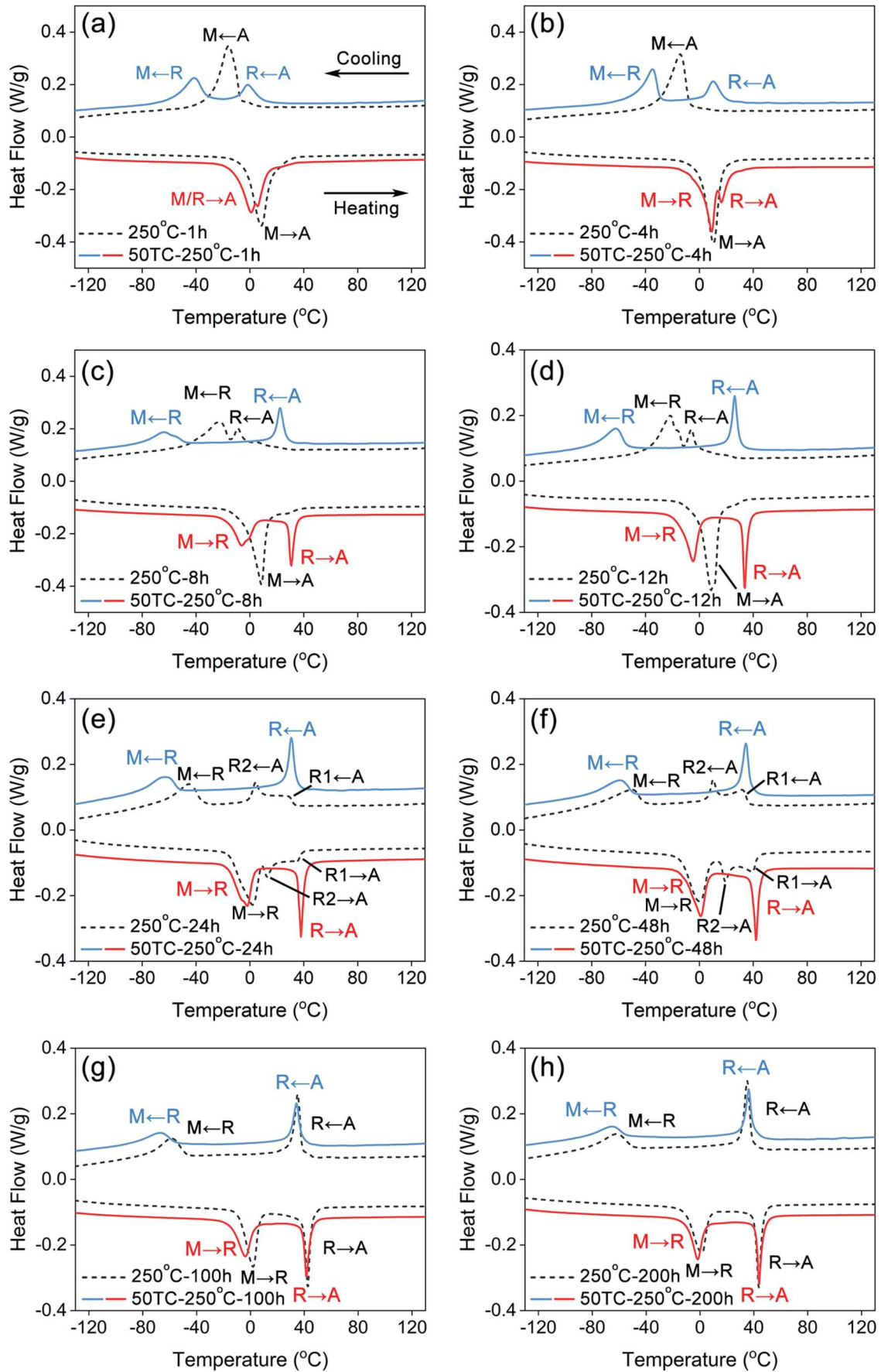
Figure 5. Phase transformation behaviour of 50 times thermal cycling treated (50TC) samples aged at 250°C for (a) 1 h, (b) 4 h, (c) 8 h, (d) 12 h, (e) 24 h, (f) 48 h, (g) 100 h, (h) 200 h, respectively. The corresponding results for the aged samples without prior thermal cycles treatment are provided for comparison, as depicted by dashed lines.
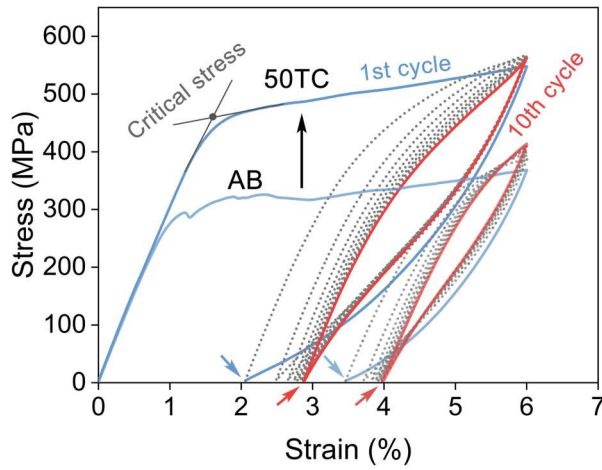
Figure 6. Ten times cyclic tensile curves of as-built (AB) and 50 times thermal cycling treated (50TC) samples to a constant strain of 6%.

improvement in superelasticity after aging for just 1 h, significantly outperforming the 1 h aged 0TC sample. The first cycle results in a residual strain of only 1.17% with a higher recovery rate of 80.50%. However, the stability of superelasticity is not sufficiently robust, as evidenced by a substantial accumulation of residual strain during subsequent cycles. Particularly, the residual strain generated at the 2nd, 3rd, and 4th cycles are 0.58%, 0.27%, and 0.14%, respectively. After 10 cycles, the accumulated residual strain escalates to 2.43%, and the recovery rate correspondingly decreases to 59.50%.

Upon extending the aging time to 4 h (Figure 7(b*)), the superelasticity of the 0TC sample remains relatively poor, with a recovery rate of only 44.67% after 10 cycles. In contrast, the 50TC sample exhibits further enhancement in superelasticity after aging for 4 h (Figure 7(b)), with the residual strain less than 1% after
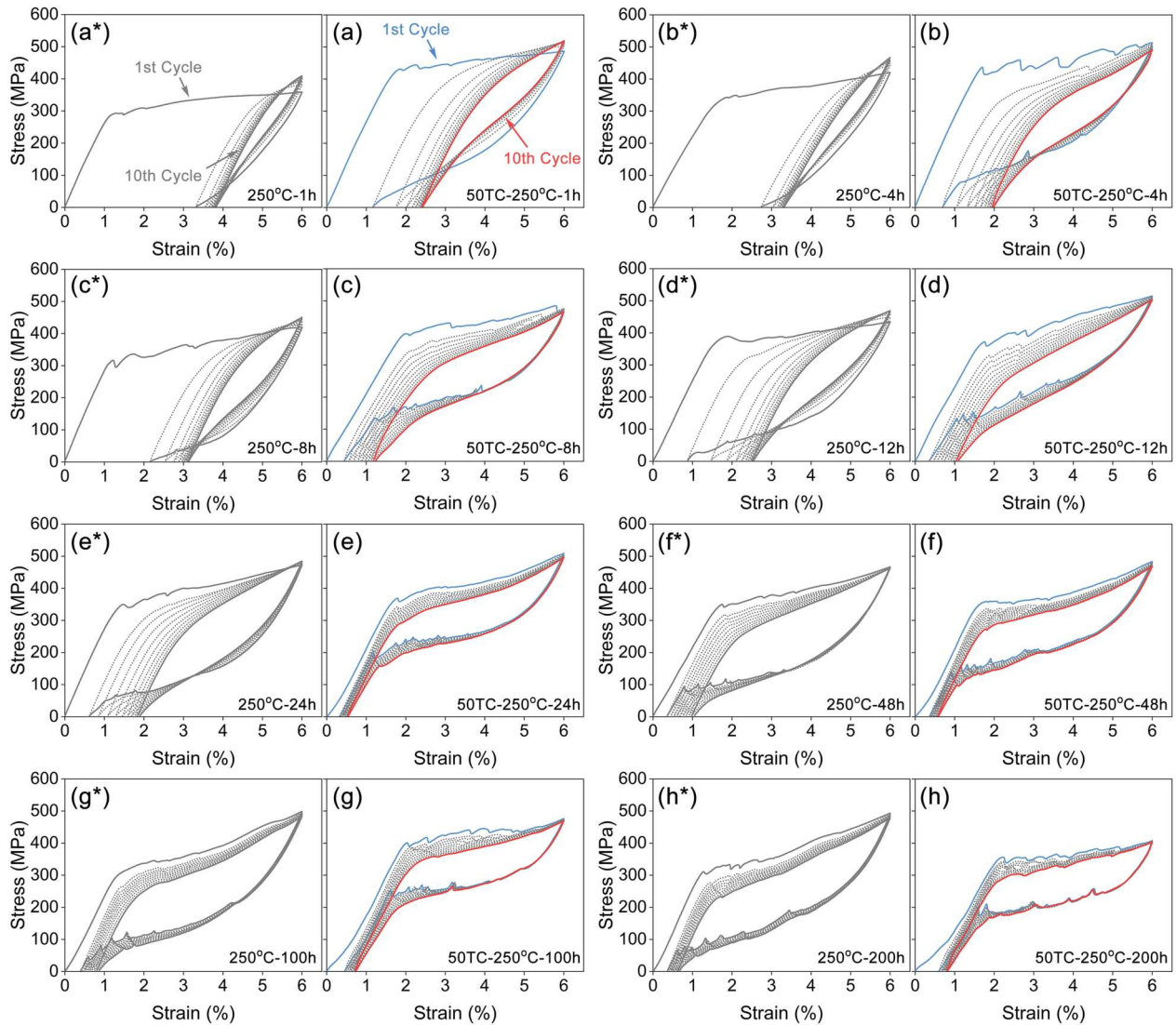

Figure 7. Ten times cyclic tensile curves to a constant strain of 6% of 50 times thermal cycling treated (50TC) samples aged at 250°C for (a) 1 h, (b) 4 h, (c) 8 h, (d) 12 h, (e) 24 h, (f) 48 h, (g) 100 h, (h) 200 h, respectively. The corresponding aged samples without thermal cycle are provided for comparison, as plotted by gray lines and shown in (a*–h*), respectively.
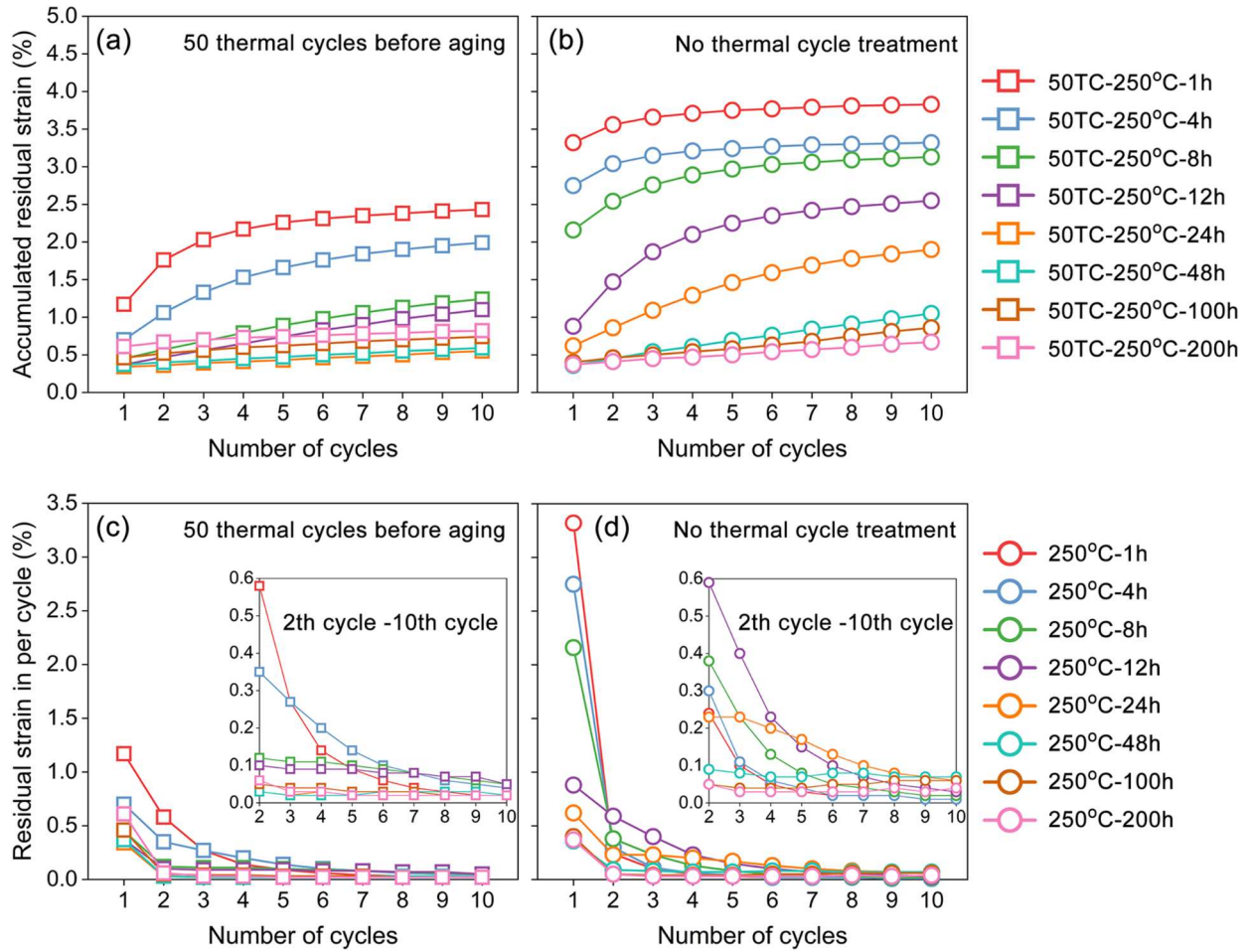
Figure 8. (a, b) The accumulated residual strain after per cycle and (c, d) the incremental residual strain in per cycle during the cyclic tensile test for all 250°C aged samples (a, c) with prior 50 thermal cycles and (b, d) without thermal cycle.

the first cycle and an increased recovery rate of 88.33%. Despite this improvement, the accumulation of residual strain is still notable in subsequent cycles, culminating in a recovery rate of 66.83% after 10 cycles.

After aging for 8 h (Figure 7(c*)), the superelastic performance of 0TC sample shows some improvement. After the first cycle, the sample shows a recovery rate of 64%. However, the recovery rate is rapidly degenerated to 47.83% after 10 cycles. Figure 7(c) shows that the superelasticity of 8 h aged 50TC sample continues to improve, with a small residual strain of 0.45% after the first cycle and a remarkable recovery rate of 92.50%. During subsequent cycles, the stability of the superelasticity is also improved and the increase of residual strain in per cycle is almost below 0.1%. This leads to the 8 h aged 50TC sample maintains a relatively high recovery rate of about 79.33% after 10 cycles.

Upon further extending the aging time to 12 h (Figure 7(d*)), the superelasticity of 0TC sample experiences a more pronounced improvement, with a recovery rate for the first cycle increased to 85.33%. The recovery

rate then decreases to 57.50% after 10 cycles. However, it is noteworthy that such performance is comparable to that of the 50TC sample aged merely for 1 h. Meanwhile, as shown in Figure 7(d), the 12 h aged 50TC sample exhibits an excellent recovery rate of 93.83% after the first cycle, and the increase of residual strain in per subsequent cycle is almost consistently maintained below 0.1%, leading to a recovery rate of 81.67% after 10 cycles.

When the aging duration comes to 24 h (Figure 7(e*)), the superelasticity of 0TC sample shows significant improvement. The recovery rate for the first cycle increases to 89.67%. However, the stability of superelasticity is relatively poor, as the recovery rate decreases to 68.33% after 10 cycles. The 50TC sample after aging for 24 h (Figure 7(e)) reaches a new height in its superelastic performance, with only 0.34% residual strain in the first cycle and a high recovery rate of 94.33%. The subsequent cycles exhibit outstanding stability with each cycle contributing less than 0.03% to the residual strain, which results in an accumulated residual strain

of only 0.55% after 10 cycles and a high recovery rate of 90.83%. This means that the recovery rate of the 24 h aged 50TC sample after 10 cycles is actually higher than the first cycle recovery rate of 24 h aged 0TC sample.

Subsequently, as exhibited in Figure 7(f*–h*), with the continued extension of aging time to 200 h, the superelasticity of the 0TC sample steadily improves. For 200 h aged 0TC sample (Figure 7(h*)), the first cycle exhibits an outstanding recovery rate of 93.83%, and the incremental increase in residual strain per cycle is maintained at a level of 0.03%. The recovery rate after 10 cycles is 88.83%, which is close to that of 24 h aged 50TC sample. As the aging time for the 50TC samples is extended beyond 24 h, their superelasticity appears to be stable. As shown in Figure 7(f–h), the samples aged for 48, 100, and 200 h, all show similar superelasticity to that of the samples aged for 24 h. Their recovery rates after 10 cycles are basically maintained at around 90%.

4. Discussion

4.1. Precipitation of Ni_4Ti_3 particles on dislocations

The classic solid-state phase transformation theory has indicated that dislocations, as the lattice defects, can facilitate the nucleation of second phase particles through providing additional energy and sites [36]. However, it need be pointed that there is an inherently low dislocation content in the EB-DED processed NiTi alloys. Based on the thermal history recorded on the substrate during the deposition process, as provided in Figure S1, it is found that the temperature during deposition is maintained above 600°C from the third layer onwards. Such high building temperature and resulted low cooling rate will not lead to high-density dislocations. Moreover, prior to aging treatment, a high-temperature solution treatment above 700°C is necessary to promote the uniformity of the microstructure [33], during which the dislocations will be further annihilated. The phase transformation behaviour and superelastic response of as-built samples directly aged at 250° C for 24 and 48 h, without solution treatment and thermal cycling treatment, are also tested, as provided in Figure S2. The results confirm that under identical aging conditions, the thermomechanical response of the as-printed samples subjected to direct aging is similar to that of the samples aged after solution treatment.

In this work, a high density of dislocations is introduced into EB-DED processed NiTi alloys by repeated martensitic phase transformation through 50 times thermal cycling treatment. Utilising the characteristic of dislocations to promote the nucleation of second phase particles, the process of precipitating Ni_4Ti_3 phase during low temperature aging is accelerated, thereby enhancing the efficiency of improving tensile superelasticity.

However, observing the Ni_4Ti_3 precipitates after low temperature aging is challenging due to the small size and coherence with the matrix. The microstructure of the 50TC sample aged at 250°C for 24 h was studied using TEM, as shown in Figure 9. Firstly, a significant amount of R-phase with distinct orientation is observed in the sample (Figure 9(a)). Additionally, numerous black spots and dislocations are noticeable on the matrix (Figure 9(b and c)). It appears that the density of precipitates is higher around the TiC phase (Figure 9(d)). According to Figure 9(e), the selected-area electron diffraction (SAED) pattern shows coexisting diffraction spots of B2 matrix, R phase and Ni_4Ti_3 phase, confirming the precipitation of Ni_4Ti_3 particles. However, the outline of the Ni_4Ti_3 particles cannot be distinctly resolved in dark-field and HRTEM image (Figure 9(f)). Their sizes should be in the range of several nanometers. Therefore, it is challenging to visually analyze the precipitation and distribution patterns of Ni_4Ti_3 particles during low-temperature aging using TEM. According to previous work on conventional NiTi alloys, Kim and Miyazaki found that the size of the formed Ni_4Ti_3 phase is only 5 nm after aging at 200°C for 3000 h and hardly larger than 15 nm after aging at 300°C for 500 h [28]. Wang et al. observed the Ni_4Ti_3 phase in a 1.7 µm grain-sized NiTi alloy after aging at 250°C for 8 h using HRTEM, revealing only the locally deformed character of the lattice [38]. They performed the fast Fourier transform (FFT) and removed the lattice spots of the B2 matrix from the FFT pattern, the corresponding Fourier-filtered image shows the lattice deformations caused by the formation of Ni_4Ti_3 nanoprecipitates. The strained B2 matrix surrounding the Ni_4Ti_3 particles causes blurring in the HRTEM image, making it hard to clearly observe the morphology of Ni_4Ti_3 particles.

In order to visually study the promoting effect of high-density dislocations on the precipitation of Ni_4Ti_3 particles during aging treatments, 0TC and 50TC samples were subjected to different aging durations (1, 4, 8, 24 h) at a high aging temperature of 450°C, which could introduce Ni_4Ti_3 particles with large size [35], thus making observation easier. The precipitates in each sample can be directly observed under SEM, as presented in Figure 10.

After aging at 450°C for 1 h (Figure 10(a and b)), only the original TiC particles are seen in the 0TC sample, with
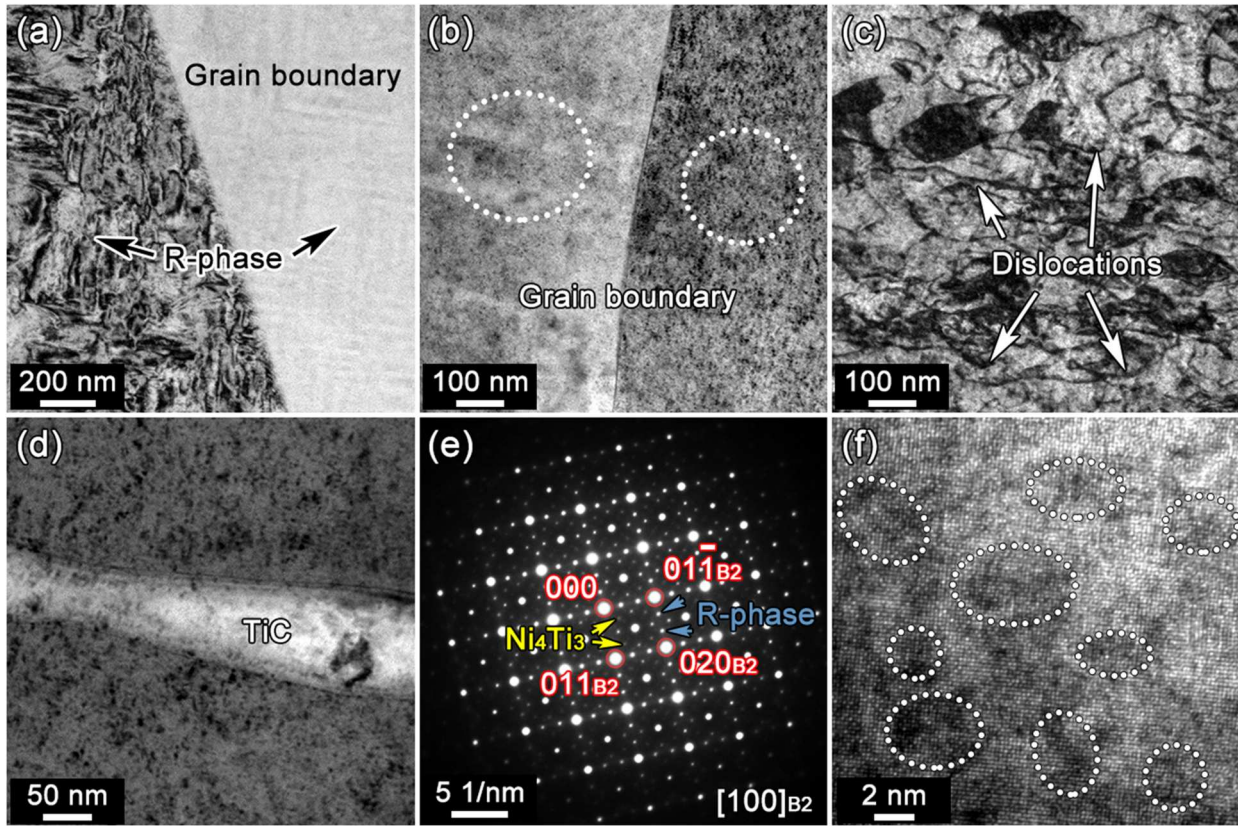
Figure 9. TEM images of 50 times thermal cycling treated sample after aging at 250°C for 24h: (a) R-phase; (b) grain boundary; (c) dislocations; (d) TiC phase; (e) SAED pattern including coexisting diffraction spots of B2 matrix, R phase and Ni_4Ti_3 phase; (f) high-resolution TEM image.

no sign of the Ni_4Ti_3 phase. In contrast, in the 50TC sample (Figure 10(c and d), a significant amount of Ni_4Ti_3 particles can be observed, exhibiting a relatively uniform distribution and small size, approximately 50 nm. When aging at 450°C for 4 h (Figure 10(e and f), a small amount of Ni_4Ti_3 particles, approximately 150 nm in size, is observed near TiC particles in the 0TC sample, while no significant Ni_4Ti_3 phase is found on the matrix away from TiC phase. In the case of the 50TC sample (Figure 10 g and 10 h), the content of the Ni_4Ti_3 particles shows some increase after 4 h of aging, with no significant change in size. After prolonging the aging time to 8 h (Figure 10(i and j), in the 0TC sample, Ni_4Ti_3 phase continues to precipitate primarily near TiC phase, with the size increasing to 350 nm. For 50TC sample (Figure 10(k and l), the precipitation of Ni_4Ti_3 particles remains uniform and their size slightly increases to 80 nm. After 24 h of aging at 450°C (Figure 10(m and n), the 0TC sample also exhibits uniform precipitation of Ni_4Ti_3 particles, with sizes around 400 nm. In the 50TC sample (Figure 10(o and p)), the size of the homogeneous Ni_4Ti_3 phase is around 150 nm.

Overall, with increasing aging time, the distribution of Ni_4Ti_3 particles in the 0TC sample has transitioned from uneven to uniform, while the 50TC sample consistently shows uniform precipitation and has a relatively large amount of precipitates in a shorter time. The size of Ni_4Ti_3 in the 0TC sample grows from 150 to 400 nm, whereas in the 50TC sample, the size increases from only 50 to 150 nm. Under the same aging time, the size of Ni_4Ti_3 in the 50TC sample is significantly smaller than that in the 0TC sample.

Therefore, it can be confirmed that the high-density dislocations introduced by 50 thermal cycles could not only significantly accelerate the nucleation of Ni_4Ti_3 phase and promote its uniform distribution during low temperature aging treatment, but also could restrict the growth of Ni_4Ti_3, which are advantageous for enhancing the matrix strength and improving the superelasticity. Obviously, this is because the high-density dislocations provide more nucleation sites, leading to a rapid and abundant formation of Ni_4Ti_3. The intensified competition in growth of Ni_4Ti_3 particles results in smaller particle sizes. Furthermore, the stress field around dislocations may also impedes the growth of Ni_4Ti_3 particles [39–41].
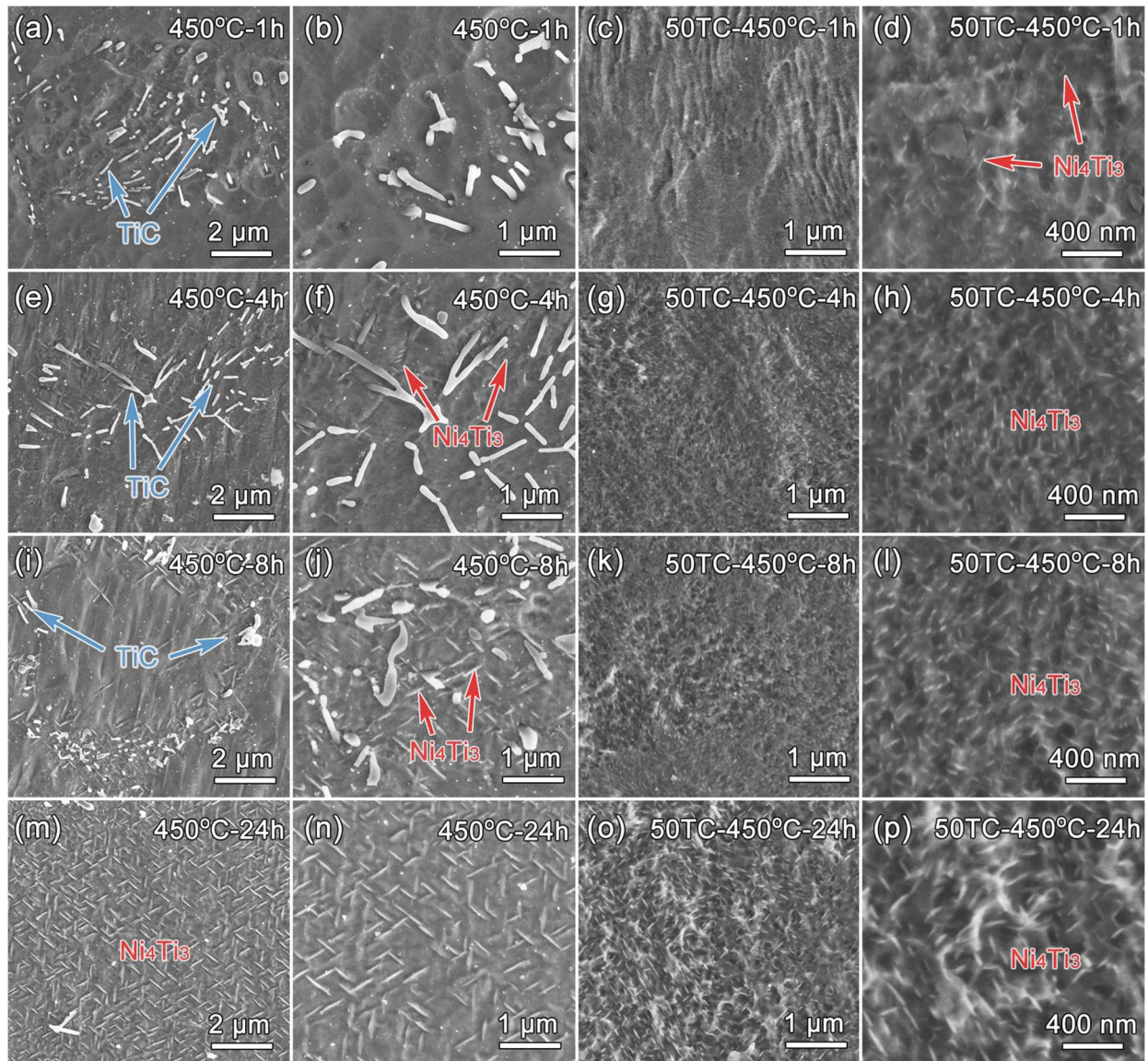
Figure 10. SEM images of samples (a, b, e, f, i, j, m, n) without thermal cycles and (c, d, g, h, k, l, o, p) with 50 thermal cycles (50TC) aged at 450℃ for (a–d) 1 h, (e–h) 4 h, (i–l) 8 h, (m–p) 24 h, respectively.

4.2. Evolution of phase transformation behaviour

The changes in the microstructure of EB-DED processed NiTi alloys resulting from the heat treatment are accompanied by the evolution of phase transformation behaviour. After 50 thermal cycles, the B19′ transformation temperature decreases, and a peak corresponding to the R-phase transformation appears. This is because the introduction of high-density dislocations hinders lattice distortions associated with the martensitic phase transformation. This hindrance has a significant impact on the B19′ transformation involving large lattice distortion, but has a smaller effect on transformation with small lattice distortions, like R-phase

transformation [42]. Therefore, the transformation sequence will change from A→M into A→R→M.

For 0TC sample, during aging at 250℃ for 1–4 h, there is no change in the phase transformation sequence, indicating the absent of Ni_4Ti_3 precipitates. Between 8 and 12 h, a weak R-phase transformation peak emerges during the cooling stage, indicating the presence of Ni_4Ti_3 particles, which impedes the martensitic phase transformation and leads to the appearance of A→R.

Within 24–48 h, a three-stage martensitic phase transformation occurs, with closely spaced two-stage R-phase transformations, while the B19′ peak is suppressed to a very low temperature. This is due to the nonuniform distribution of Ni_4Ti_3 particles within the grains, where in

specific regions, a considerable amount Ni_4Ti_3 precipitates, causing the A→R1 transformation to occur first, while in certain areas where the precipitation is minimal, the A→R2 transformation follows. This kind of three-stage martensitic phase transformation is also frequently reported in conventional coarse-grained NiTi alloys after aging at 250°C for specific durations [43–45]. Due to the preferential formation of Ni_4Ti_3 at grain boundaries, the uneven distribution of Ni_4Ti_3 at grain boundaries and within grains results in the first-stage R-phase transformation occurring at the grain boundaries, followed by the second-stage R-phase transformation within the grains.

After aging for 100–200 h, the overall three-stage phase transformation of 0TC samples converts to a two-stage phase transition, the corresponding two-stage R phase transformation changes into one-stage, and the phase transformation behaviour begins to stabilise. This indicates the distribution of Ni_4Ti_3 precipitates within the grains is uniform.

For the 50TC samples, we observed that during aging at 250°C for 1–4 h, a distinct single-stage R phase emerges, with a difference of about 40°C between Mp and Rp. After aging for 8–12 h, the difference between Mp and Ap continues to expand to 95°C around, and the phase transformation sequence begins to stabilise at this point. The phase transformation temperatures also remain essentially unchanged until 200 h aging.

During the aging of 50TC samples from 1 to 200 h at 250°C, only a two-stage martensitic transformation containing one-stage R phase transformation occurs. There is no occurrence of a three-stage transformation involving two-stage R phase transformation. Additionally, the phase transformation behaviour stabilises starting at 8 h, exhibiting the same phase transformation behaviour as exhibited in the 0TC sample after 100–200 h of aging. This well demonstrates the Ni_4Ti_3 particles could uniformly precipitate within the matrix in a relatively short period of time.

This work also evaluated the phase transformation behaviour of the 450°C aged samples used previously to assist in observing the distribution of Ni_4Ti_3, as shown in Figure 11. It can be observed that the 0TC sample aged for 1–4 h still maintains a one-stage martensitic transformation, consistent with the almost negligible precipitation of Ni_4Ti_3 confirmed under SEM (Figure 11(a and b)). After aging for 8 h (Figure 11(c)), a three-stage martensitic transformation appears, which is also attributed to the uneven distribution of Ni_4Ti_3 particles, as found under SEM where they are distributed primarily around the original TiC particles. At 24 h (Figure 11(d)), a two-stage martensitic transformation begins, agreeing with the observation of uniformly distributed Ni_4Ti_3.

However, the 50TC samples (Figure 11(a–d)), almost exhibit a two-stage martensitic transformation from aging for only 1 h, similar to that of the 0TC sample aged for 24 h. This is consistent with the SEM observation of uniformly precipitated Ni_4Ti_3 phase from 1 h onwards. Therefore, the analysis of the phase transformation behaviour effectively confirms that the high-density dislocations introduced by thermal cycles significantly accelerate the uniform precipitation of Ni_4Ti_3 particles within the grains. Moreover, it also enables the NiTi alloy to avoid the occurrence of complex three-stage phase transformation, simplifying the evolution of phase transformation behaviour and significantly accelerating the stability of phase transformation temperatures and sequence, which is of great significance for the practical application.

4.3. Accelerated improvement in tensile superelasticity

As mentioned above, the excellent superelasticity of the 50TC sample obtained through aging at 250°C for just 24 h reaches the same level as that of the 0TC sample after 200 h of aging, meaning a huge improvement in aging efficiency. During the superelastic test to a constant tensile strain of 6%, the first cycle achieves a recovery rate of approximately 95%, while the superelastic recovery rate after 10 cycles can still be maintained at 90%. This essentially represents the best superelasticity achieved by additively manufactured of NiTi alloys to date.

Evidently, this can also be attributed to the introduction of dislocations by thermal cycling, which greatly accelerates the uniform precipitation of nano Ni_4Ti_3 particles. The classical theory of NiTi alloys has well demonstrated the excellent strengthening effect of the nano Ni_4Ti_3 particles on the matrix and their significant ability to improve superelasticity [17,18,37]. Therefore, thermal cycling can expedite the improvement in superelasticity during subsequent low-temperature aging treatment.

In order to further evaluate the advantages of thermal cycling coupled with low-temperature aging for improving superelasticity, this work further provides a comparison with conventional NiTi alloy sheets. The selected Ti-50.8 at.% Ni alloy sheet has a thickness of 0.5 mm and achieves a fully equiaxed grain structure after annealing, with an average grain size of 12 μm. The superelasticity of NiTi alloy sheet after 24 h of aging at 250°C is compared with that of the 0TC and 50TC samples under the same aging condition, as illustrated in Figure 12. It can be found that the 24 h aged NiTi alloy sheet exhibits typical superelastic behaviour under cyclic loading at a
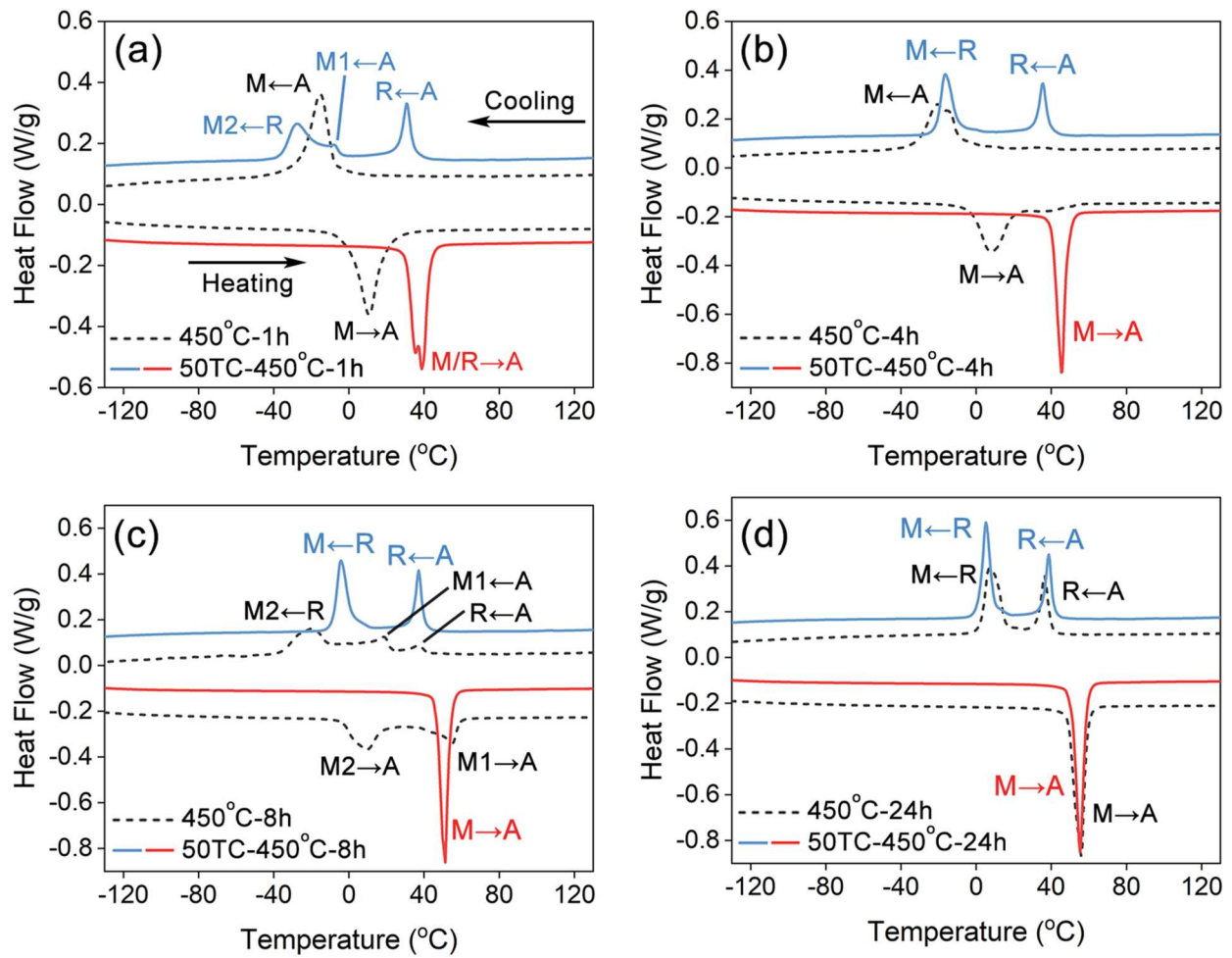
Figure 11. Phase transformation behaviour of 50 times thermal cycling treated (50TC) samples aged at 450°C for (a) 1 h, (b) 4 h, (c) 8 h, (d) 24 h, respectively. The corresponding aged samples without thermal cycle are provided for comparison, as depicted by dashed lines.
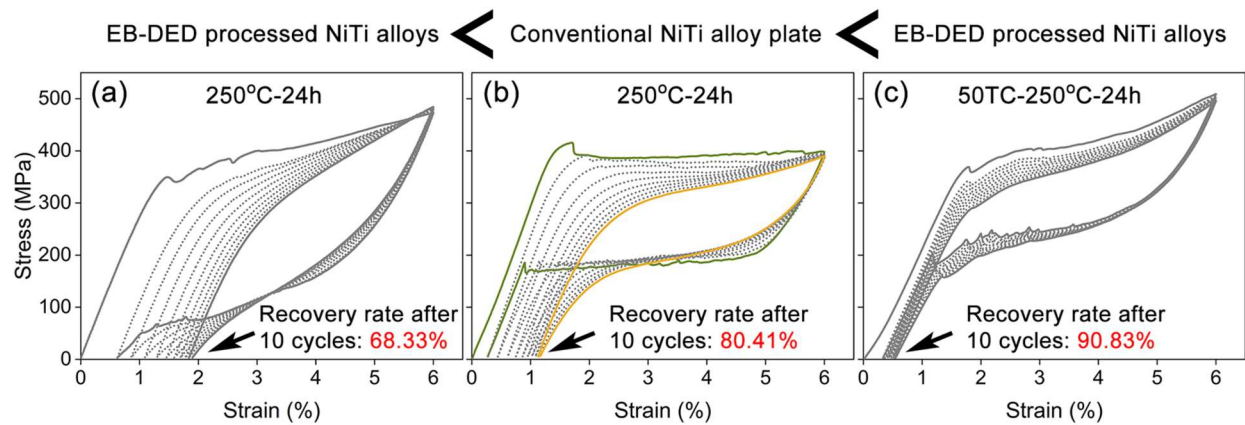

Figure 12. Ten times cyclic tensile curves of (a) EB-DED processed NiTi alloys without thermal cycling treatment, (b) conventional NiTi alloy plate, (c) EB-DED processed NiTi alloys with 50 times thermal cycling treatment, after aging at 250°C for 24 h. The conventional NiTi alloy plate are fully annealed with with an average grain size of 12 μm.

tensile strain of 6%. The recovery rate after 10 cycles is 80.41%, which is obviously better than that of 0TC sample without thermal cycling treatment (68.33%).

Different from the larger grain size in 0TC sample, the presence of smaller equiaxed grains in NiTi alloy sheet provides more grain boundaries to promote the
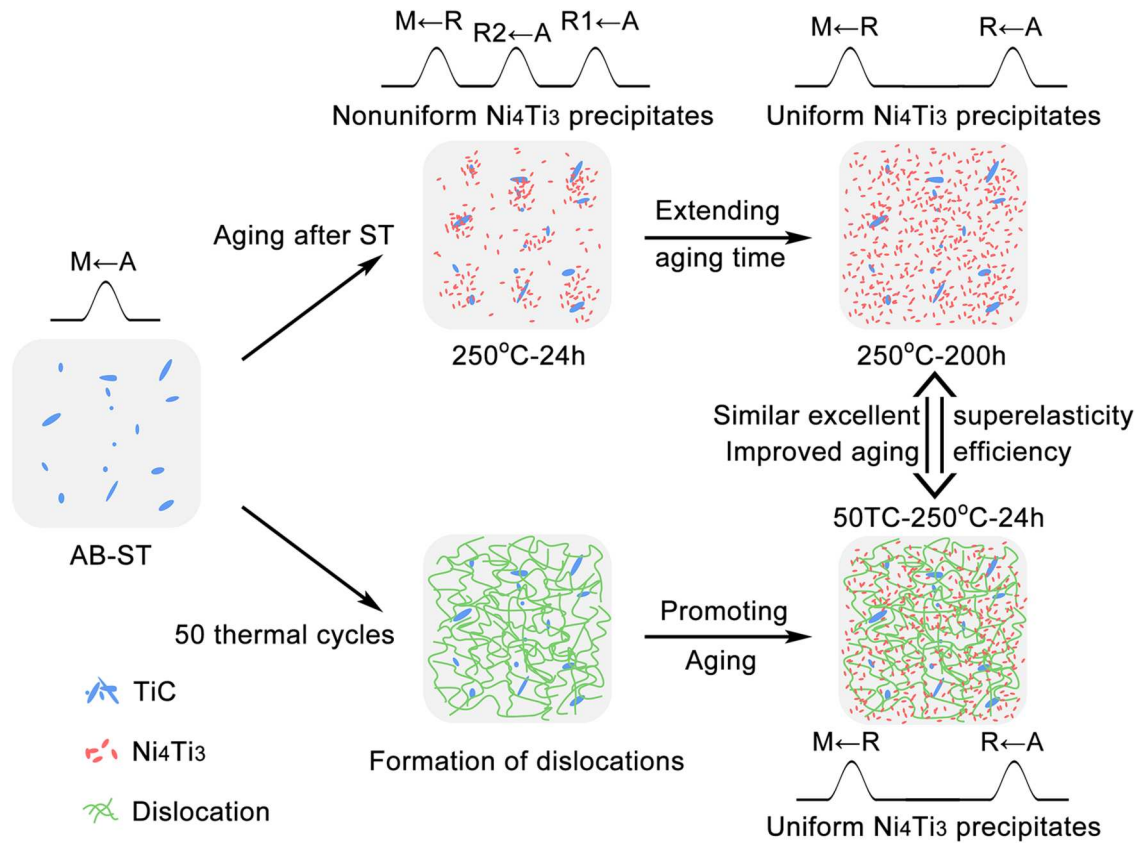
Figure 13. Schematic diagram of accelerated precipitation of Ni_4Ti_3 particles by introduction of dislocations through thermal cycling treatment.

nucleation of nano Ni_4Ti_3 particles, thereby resulting in better superelasticity under the same aging conditions.

However, the superelasticity of the 24 h aged 50TC sample is superior to that of the conventional NiTi alloy sheet, 10% higher in recovery rate after 10 cycles. This indicates that the introduction of high-density dislocations through thermal cycling effectively compensates for the adverse effects of coarse grains in EB-DED processed NiTi alloys on low-temperature aging efficiency.

Overall, this study demonstrates that the combined heat treatment of thermal cycling and low-temperature aging can quickly and effectively improve the superelasticity of NiTi alloys fabricated by EB-DED, as schematically shown in Figure 13. This low-cost and high-efficiency heat treatment method is of significant importance for the practical application of NiTi alloys prepared by EB-DED, which also has important implications for the NiTi alloys produced by other additive manufacturing techniques.

5. Conclusions

This study investigates the influence of artificial thermal cycling treatment coupled with low-temperature aging

treatment on the microstructure, phase transformation behaviour, and tensile superelasticity of NiTi alloys fabricated by EB-DED. The main conclusions are as follows:

(1) The high-density dislocations are successfully introduced through 50 thermal cycles before aging treatment. The nano-sized Ni_4Ti_3 particles precipitated at 250°C are too small (<10 nm) to be clearly observed. By conducting high-temperature aging at 450°C, the large-sized Ni_4Ti_3 precipitates can be observed. It is found that the high-density dislocations not only promote the homogeneous precipitation of Ni_4Ti_3 during the low-temperature aging process but also constrain the growth of Ni_4Ti_3, resulting in a reduction in precipitate size.

(2) Prior thermal cycling treatment can accelerate the stabilisation of phase transformation behaviour after low-temperature aging. During the aging process, the thermal cycling treated samples always demonstrate a two-stage martensitic phase transformation involving a one-stage R-phase transformation. Aging for 8 h is sufficient to obtain stable phase transformation behaviour, achieving the same level of stability as that of samples aged for 100 h

without prior thermal cycling. It well circumvents the complex evolution of phase transformation sequences and temperatures during the low-temperature aging process of samples without thermal cycling.

(3) The combination of thermal cycling treatment and low-temperature aging treatment can achieve a rapid and effective improvement in tensile superelasticity. The sample with 50 thermal cycles can achieve excellent tensile superelasticity after aging at 250°C for 24 h. In a 6% tensile superelastic test, the recovery rate after the first cycle is as high as around 95%, and even after 10 cycles, the recovery rate can still be maintained at over 90%. This represents nearly the best tensile superelasticity for additively manufactured NiTi alloys, and comparable to the performance of 200 h aged sample without prior thermal cycle.

Disclosure statement

No potential conflict of interest was reported by the author(s).

Funding

Data availability statement

The data that support the findings of this study are available from the corresponding author upon reasonable request.

References

[1] Otsuka K, Ren X. Physical metallurgy of Ti–Ni-based shape memory alloys. Prog Mater Sci. 2005;50:511–678. doi:10.1016/j.pmatsci.2004.10.001

[2] Fadlallah SA, El-Bagoury N, Gad El-Rab SMF, et al. An overview of NiTi shape memory alloy: corrosion resistance and antibacterial inhibition for dental application. J Alloys Compd. 2014;583:455–464. doi:10.1016/j.jallcom.2013.08.029

[3] Bansiddhi A, Sargeant TD, Stupp SI, et al. Porous NiTi for bone implants: a review. Acta Biomater. 2008;4:773–782. doi:10.1016/j.actbio.2008.02.009

[4] Xi R, Jiang H, Li G, et al. In-situ alloying of NiTiNb ternary shape memory alloys via laser powder bed fusion using pre-alloyed NiTi and elemental Nb powders: microstructure, phase transformation behavior and functional properties. Addit Manuf. 2024;79:103933. doi:10.1016/j.addma.2023.103933

[5] Mohd Jani J, Leary M, Subic A, et al. A review of shape memory alloy research, applications and opportunities. Mater Des. 2014;56:1078–1113. doi:10.1016/j.matdes.2013.11.084

[6] Elahinia M, Shayesteh Moghaddam N, Taheri Andani M, et al. Fabrication of NiTi through additive manufacturing: a review. Prog Mater Sci. 2016;83:630–663. doi:10.1016/j.pmatsci.2016.08.001

[7] Xi R, Jiang H, Kustov S, et al. Influence of Nb addition and process parameters on the microstructure and phase transformation behavior of NiTiNb ternary shape memory alloys fabricated by laser powder bed fusion. Scr Mater. 2023;222:114996. doi:10.1016/j.scriptamat.2022.114996

[8] Herzog D, Seyda V, Wycisk E, et al. Additive manufacturing of metals. Acta Mater. 2016;117:371–392. doi:10.1016/j.actamat.2016.07.019

[9] Wang K, Liu W, Li X, et al. Effect of hot isostatic pressing on microstructure and properties of high chromium K648 superalloy manufacturing by extreme high-speed laser metal deposition. J Mater Res Technol. 2024;28:3951–3959. doi:10.1016/j.jmrt.2023.12.280

[10] Weinert K, Petzoldt V. Machining of NiTi based shape memory alloys. Mater Sci Eng A. 2004;378:180–184. doi:10.1016/j.msea.2003.10.344

[11] Oliveira JP, Miranda RM, Braz Fernandes FM. Welding and joining of NiTi shape memory alloys: A review. Prog Mater Sci. 2017;88:412–466. doi:10.1016/j.pmatsci.2017.04.008

[12] Xi R, Jiang H, Li G, et al. Effect of solution treatment on the microstructure, phase transformation behavior and functional properties of NiTiNb ternary shape memory alloys fabricated via laser powder bed fusion in-situ alloying. Int J Extrem Manuf. 2024;6:045002. doi:10.1088/2631-7990/ad35fc

[13] Lu HZ, Ma HW, Cai WS, et al. Stable tensile recovery strain induced by a Ni4Ti3 nanoprecipitate in a Ni50.4Ti49.6 shape memory alloy fabricated via selective laser melting. Acta Mater. 2021;219:117261. doi:10.1016/j.actamat.2021.117261

[14] Saedi S, Turabi AS, Taheri Andani M, et al. The influence of heat treatment on the thermomechanical response of Ni-rich NiTi alloys manufactured by selective laser melting. J Alloys Compd. 2016;677:204–210. doi:10.1016/j.jallcom.2016.03.161

[15] Wang X, Kustov S, Van Humbeeck J. A short review on the microstructure, transformation behavior and functional properties of NiTi shape memory alloys fabricated by selective laser melting. Materials (Basel). 2018;11:1683. doi:10.3390/ma11091683

[16] Malard B, Pilch J, Sittner P, et al. Microstructure and functional property changes in thin Ni-Ti wires heat treated by electric current — high energy x-ray and tem investigations. Funct Mater Lett. 2009;02:45–54. doi:10.1142/S1793604709000557

[17] Wang X, Kustov S, Li K, et al. Effect of nanoprecipitates on the transformation behavior and functional properties of a Ti–50.8 at.% Ni alloy with micron-sized grains. Acta Mater. 2015;82:224–233. doi:10.1016/j.actamat.2014.09.018

[18] Chen H, Xiao F, Liang X, et al. Improvement of the stability of superelasticity and elastocaloric effect of a Ni-rich Ti-Ni

alloy by precipitation and grain refinement. Scr Mater. 2019;162:230–234. doi:10.1016/j.scriptamat.2018.11.024

[19] Prokoshkin SD, Khmelevskaya IY, Dobatkin SV, et al. Alloy composition, deformation temperature, pressure and post-deformation annealing effects in severely deformed Ti–Ni based shape memory alloys. Acta Mater. 2005;53:2703–2714. doi:10.1016/j.actamat.2005.02.032

[20] Tong YX, Guo B, Chen F, et al. Thermal cycling stability of ultrafine-grained TiNi shape memory alloys processed by equal channel angular pressing. Scr Mater. 2012;67:1–4. doi:10.1016/j.scriptamat.2012.03.005

[21] Delville R, Malard B, Pilch J, et al. Transmission electron microscopy investigation of dislocation slip during super-elastic cycling of Ni–Ti wires. Int J Plasticity. 2011;27:282–297. doi:10.1016/j.ijplas.2010.05.005

[22] Chen J, Lei L, Fang G. Grain-size effects on the temperature-dependent elastocaloric cooling performance of polycrystalline NiTi alloy. J Alloys Compd. 2022;927:166951. doi:10.1016/j.jallcom.2022.166951

[23] Zeng Z, Cong BQ, Oliveira JP, et al. Wire and arc additive manufacturing of a Ni-rich NiTi shape memory alloy: microstructure and mechanical properties. Microstruct Mech Properties, Addit Manuf. 2020;32:101051. doi:10.1016/j.addma.2020.101051

[24] Li B, Wang L, Wang B, et al. Solidification characterization and its correlation with the mechanical properties and functional response of NiTi shape memory alloy manufactured by electron beam freeform fabrication. Addit Manuf. 2021;48:102468. doi:10.1016/j.addma.2021.102468

[25] Zhou Q, Hayat MD, Chen G, et al. Selective electron beam melting of NiTi: microstructure, phase transformation and mechanical properties. Mater Sci Eng A. 2019;744:290–298. doi:10.1016/j.msea.2018.12.023

[26] Xi R, Jiang H, Li G, et al. Effect of Fe addition on the microstructure, transformation behaviour and superelasticity of NiTi alloys fabricated by laser powder bed fusion. Virtual Phys Prototyp. 2023;18:e2126376. doi:10.1080/17452759.2022.2126376

[27] Karaca HE, Saghaian SM, Ded G, et al. Effects of nanoprecipitation on the shape memory and material properties of an Ni-rich NiTiHf high temperature shape memory alloy. Acta Mater. 2013;61:7422–7431. doi:10.1016/j.actamat.2013.08.048

[28] Kim JI, Miyazaki S. Effect of nano-scaled precipitates on shape memory behavior of Ti-50.9at.%Ni alloy. Acta Mater. 2005;53:4545–4554. doi:10.1016/j.actamat.2005.06.009

[29] Feng B, Wang C, Zhang Q, et al. Effect of laser hatch spacing on the pore defects, phase transformation and properties of selective laser melting fabricated NiTi shape memory alloys. Mater Sci Eng A. 2022;840:142965. doi:10.1016/j.msea.2022.142965

[30] Gu D, Ma C. In-situ formation of Ni4Ti3 precipitate and its effect on pseudoelasticity in selective laser melting additive manufactured NiTi-based composites. Appl Surf Sci. 2018;441:862–870. doi:10.1016/j.apsusc.2018.01.317

[31] Zhang M, Fang X, Wang Y, et al. High superelasticity NiTi fabricated by cold metal transfer based wire arc additive

manufacturing. Mater Sci Eng A. 2022;840:143001. doi:10.1016/j.msea.2022.143001

[32] Pu Z, Du D, Zhang D, et al. Study on the role of carbon in modifying second phase and improving tensile properties of NiTi shape memory alloys fabricated by electron beam directed energy deposition. Additive Manuf. 2023;75:103733. doi:10.1016/j.addma.2023.103733

[33] Pu Z, Du D, Wang K, et al. Microstructure, phase transformation behavior and tensile superelasticity of NiTi shape memory alloys fabricated by the wire-based vacuum additive manufacturing. Mater Sci Eng A. 2021;812:141077. doi:10.1016/j.msea.2021.141077

[34] Dutkiewicz J, Rogal Ł, Kalita D, et al. Microstructure, mechanical properties, and martensitic transformation in NiTi shape memory alloy fabricated using electron beam additive manufacturing technique. J Mater Eng Perform. 2022.

[35] Pu Z, Du D, Zhang D, et al. Improvement of tensile superelasticity by aging treatment of NiTi shape memory alloys fabricated by electron beam wire-feed additive manufacturing. J Mater Sci Technol. 2023;145:185–196. doi:10.1016/j.jmst.2022.10.050

[36] Christian J. *The theory of transformations in metals and alloys*. Newnes; 2002.

[37] Gall K, Maier HJ. Cyclic deformation mechanisms in precipitated NiTi shape memory alloys. Acta Mater. 2002;50:4643–4657. doi:10.1016/S1359-6454(02)00315-4

[38] Wang X, Li K, Schryvers D, et al. R-phase transition and related mechanical properties controlled by low-temperature aging treatment in a Ti–50.8at.% Ni thin wire. Scr Mater. 2014: 21–24. doi:10.1016/j.scriptamat.2013.10.006

[39] Chen L, Li J, Zhang Y, et al. Effect of low-temperature pre-deformation on precipitation behavior and microstructure of a Zr-Sn-Nb-Fe-Cu-O alloy during fabrication. J Nucl Sci Technol. 2016;53:496–507. doi:10.1080/00223131.2015.1059776

[40] Ham FS. Stress-Assisted precipitation on dislocations. J Appl Phys. 1959;30:915–926. doi:10.1063/1.1735262

[41] Douin J, Donnadieu P, Epicier T, et al. Stress field around precipitates: direct measurement and relation with the behavior of dislocations. Mater Sci Eng A. 2001: 270–273. doi:10.1016/S0921-5093(01)01103-0

[42] Ren X, Miura N, Zhang J, et al. A comparative study of elastic constants of Ti–Ni-based alloys prior to martensitic transformation. Mater Sci Eng A. 2001;312:196–206. doi:10.1016/S0921-5093(00)01876-1

[43] Wang X, Verlinden B, Kustov S. Multi-stage martensitic transformation in Ni-rich NiTi shape memory alloys. Funct Mater Lett. 2017;10:1740004. doi:10.1142/S1793604717400045

[44] Zhou Y, Zhang J, Fan G, et al. Origin of 2-stage R-phase transformation in low-temperature aged Ni-rich Ti–Ni alloys. Acta Mater. 2005;53:5365–5377. doi:10.1016/j.actamat.2005.08.013

[45] Wang X, Li C, Verlinden B, et al. Effect of grain size on aging microstructure as reflected in the transformation behavior of a low-temperature aged Ti–50.8at.% Ni alloy. Scr Mater. 2013;69:545–548. doi:10.1016/j.scriptamat.2013.06.023